Three Dimensional Flow Structures in Journal Bearings

Peter STÜCKE [1*], Matthias NOBIS [2], Marcus SCHMIDT [2]

* Corresponding author: Tel.: ++49 (0)375 5363444; Fax: ++49 (0)375 5363393;
Email: peter.stuecke@fh-zwickau.de
1: Institut für Energiemanagement i. G., Westsächsische Hochschule Zwickau, Germany
2: Forschungs- und Transferzentrum, Westsächsische Hochschule Zwickau, Germany

Abstract In general, the fluid flow in journal bearings can be described by the Navier-Stokes Equations and the conservation of mass. The application of the small gap criterion allows a simplification of these equations yielding the Reynolds Equation, which links the local gap size with the pressure gradient resulting in a powerful tool for the designing process of journal bearings. Typically, the Reynolds Equation is used in EHD-design software based on FE-methods, which is used to compute pressure distributions, forces, deformations and many more parameters needed for the selection of the right bearing geometry. However, there are regions in the journal bearing where the Reynolds Equation must fail, because either the small gap criterion or the Couette flow assumption is violated. There are pockets, grooves and holes, which are necessary to distribute the oil supply across the gap. Moreover, the oil feed represents a cross flow perpendicular to the circumferential main flow. In these regions three dimensional flow structures replace the undisturbed Couette flow, which are strongly affected by vortices, but are non-turbulent due to the Re-scale. This work presents experimental data obtained from a cylinder apparatus with moderate gap sizes, which features independently rotating cylinders and a cross flow through a hole in the sidewall. LDV-measurements of velocity profiles and visualization methods to animate the three dimensional nature of the flow are presented. The experimental data are used to validate 3D-CFD calculations, which are expanded towards smaller gap sizes in the range of typical journal bearings in automotive applications.

Keywords: Micro Flow, Journal Bearing

1. Introduction

Journal bearings or dynamic fluid bearings are widely used in automotive and turbo machine applications and are classic examples of micro flow. For example, a typical bearing for an automotive 4-cylinder engine has a diameter of 40 mm and a clearance of 0.1% resulting in an average oil film thickness of 20 µm. If an eccentricity of 0.9 is assumed the minimum gap between shaft and bushing becomes 2µm.

Main, connecting rod and piston bearings of internal combustion engines are journal bearings because of their high loading capacity versus small, required construction space and their low running noise. Journal bearings are used in turbochargers, because of high rotational speeds and adverse operating conditions at design point.

In both of these applications the journal bearing must be continuously supplied with fresh oil for one to replenish the losses at the open ends of the bearing and secondly for cooling purposes. Oil supply drillings are placed in the engine body through existing structures and wherever access for the drilling machine is possible. There are no general design guidelines for the circumferential position found throughout the industry. Fig. 1 shows two examples of actual engine design. The four cylinder BMW engine has the feed hole at +45° towards the high pressure side of the bearing and the Mercedes-Benz engine has the hole at -35° towards the low pressure side. The angle is measured from the maximum gap width which typically falls in line with the vertical engine axis. The only common fact is that the holes to supply the main bearing are located in the upper half of the bearing, which is the low load section and which is facing the engine body rather than the engine pan. Here it

should be noted that main bearings provide a second function supplemental to the original support of the crank shaft. The feed oil for the connecting rod bearing is transported via a drilling inside the crank shaft from the main to the rod bearing. Thus, the main bearing is fed with a surplus amount of oil to ensure the supply of the connecting rod bearing. This flow of oil must enter the oil film inside the gap between crank shaft and bushing through the feed hole located in the bearing bushing and is then collected by the exit hole inside the shaft, which in turn connects through a diagonal drilling with the connecting rod bearing. This description illustrates the very complex flow structure, which characterizes the flow inside the lubrication film of the main bearing.

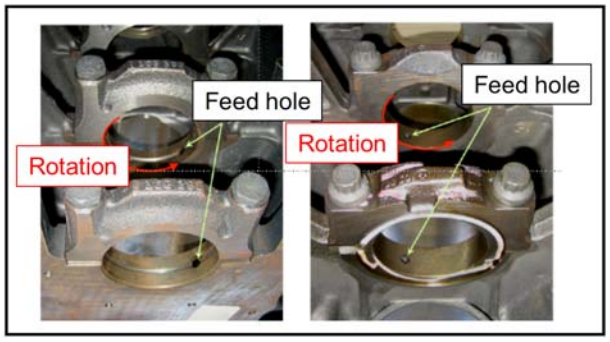

Fig. 1: design examples for main bearing oil supply hole locations, BMW left, Mercedes-Benz (right), view from the engine pan upwards

Moreover, engine test data give further evidence of the three-dimensional character of the flow adjacent to holes and other geometrical features of journal bearings. Two examples of flow induced cavitation, where the affected area is found at the very edge of the feed hole are shown in Fig. 2 and Fig. 3.

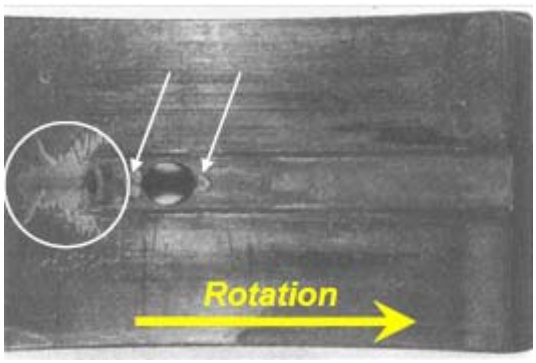

Fig. 2: cavitation damage on both sides of the feedhole and at the leading edge of the oil pocket, Berg [1]

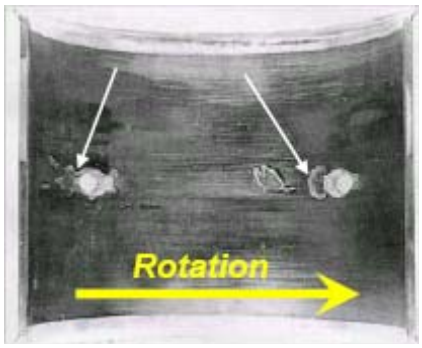

Fig. 3: cavitation damage on both sides of the feedhole, Gläser [2]

During the design process finite element methods (FEM and EHD i.e., elasto-hydrodynamics) are applied to calculate bearing loads, oil temperature, minimum gap restriction and oil flow. Typically, this method is based on a 2D flow model for narrow channels, which generates excellent results for standard applications.

However, this approach must fail at least for two reasons in the vicinity of feedholes, pockets or grooves where the oil supply enters the lubrication film between shaft and bushing. Firstly, the condition for small channel height is violated and secondly, the feed flow enters the film orthogonally from the side resulting in a fully developed three-dimensional flow. Therefore, a full 3D numerical simulation was applied to investigate the flow structures in journal bearings with cross flow. The program OpenFOAM was used to carry out the computational flow dynamics (CFD) calculations.

2. Approach

2.1 Mathematical model

A journal bearing can be regarded as a system of two circular cylinders, where the inner cylinder Z1 (i.e. shaft) rotates around the z-axis with the circumferential speed U_1 and the outer cylinder Z2 (i.e. bushing) is at rest. Fig. 4 illustrates schematically a cross section of the system.

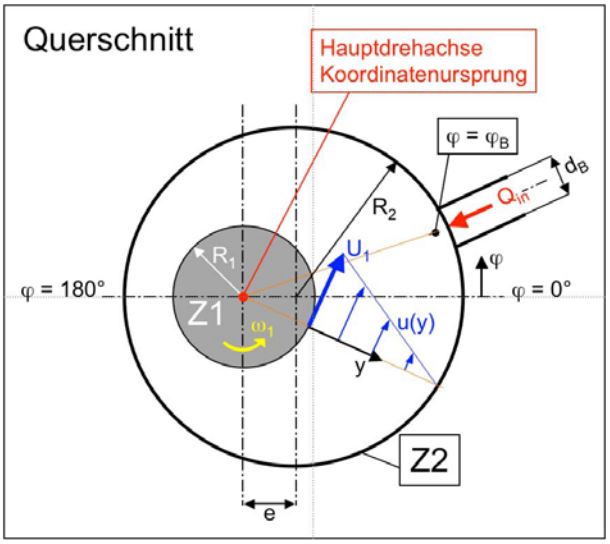

Fig. 4: cross section of the flow system

The eccentricity e denotes the distance between the cylinder axis. The angle $\varphi = 0°$ defines the widest gap. For convenience the coordinates are defined as

circumferential: $x = R_1 \varphi$
radial: $y = r - R_1$
axial: z

For the project investigating the three dimensional flow structure in journal bearings the unsteady Navier Stokes Equations (2 - 4) for incompressible fluids are solved together with the continuity equation (1) for the conservation of mass.

$$\frac{\partial u}{\partial x} + \frac{\partial v}{\partial y} + \frac{\partial w}{\partial z} = 0 \tag{1}$$

$$\frac{Du}{Dt} = -\frac{1}{\rho}\frac{\partial p}{\partial x} + \nu\left(\frac{\partial^2 u}{\partial x^2} + \frac{\partial^2 u}{\partial y^2} + \frac{\partial^2 u}{\partial z^2}\right) \tag{2}$$

$$\frac{Dv}{Dt} = -\frac{1}{\rho}\frac{\partial p}{\partial y} + \nu\left(\frac{\partial^2 v}{\partial x^2} + \frac{\partial^2 v}{\partial y^2} + \frac{\partial^2 v}{\partial z^2}\right) \tag{3}$$

$$\frac{Dw}{Dt} = -\frac{1}{\rho}\frac{\partial p}{\partial z} + \nu\left(\frac{\partial^2 w}{\partial x^2} + \frac{\partial^2 w}{\partial y^2} + \frac{\partial^2 w}{\partial z^2}\right) \tag{4}$$

For both, spatial and time resolution a second order solver is used.

If the narrow channel condition is applicable equations (1) through (4) can be reduced. This assumption is usually applied, when the flow in journal bearings is computed. In the following section this model is discussed to visualize the differences between the full 3D-approach and the simplified model, which is more common.

The continuity equations can be written for the circumferential and axial mean velocity across the gap width.

$$\frac{\partial \overline{u}}{\partial x} + \frac{\partial \overline{w}}{\partial z} = 0 \tag{5}$$

And the impulse equations yield

$$\frac{1}{\rho}\frac{\partial p}{\partial x} = \nu\frac{\partial^2 u}{\partial y^2} \tag{6}$$

$$\frac{1}{\rho}\frac{\partial p}{\partial z} = \nu\frac{\partial^2 w}{\partial y^2} \tag{7}$$

With p being only a function of (x, z) equations (6, 7) can be integrated over y resulting in the mean velocities by taking into account the boundary conditions: inner cylinder rotates with U_1 and outer cylinder is at rest.

$$\overline{u} = -\frac{h^3}{12\mu}\frac{\partial p}{\partial x} + \frac{U_1 h}{2} \tag{8}$$

$$\overline{w} = -\frac{h^3}{12\mu}\frac{\partial p}{\partial z} \tag{9}$$

Here h denotes the local gap width, which depends on the eccentricity e, but can also be expanded to include shaft bending or bushing deformation. Hence

$$h = f(x, z) \tag{10}$$

In summary, (8) and (9) are combined with (5) to become the so called Reynolds equation for journal bearings.

$$\frac{\partial}{\partial x}\left(\frac{h^3}{\mu}\frac{\partial p}{\partial x}\right) + \frac{\partial}{\partial z}\left(\frac{h^3}{\mu}\frac{\partial p}{\partial z}\right) = 6U_1\frac{\partial h}{\partial x} \tag{11}$$

Without doubt, the Reynolds equation is a strong tool for design engineers during the development process for journal bearings for internal combustion engines. However, this equation is limited to describe a two-dimensional flow, because it is an integral method that can be used to compute flow rates or mean velocities (eq. (8) and (9)) across the gap width.

Therefore it is vital to apply three-dimensional theory, if the lubrication flow shall be described and real bearing geometry is taken into consideration.

2.2 Grid generation

Careful consideration was given to the grid generation based on own experiences related

to the calculation of the critical Reynolds number, which defines the onset of Taylor vortices in the Couette flow between rotating cylinders. Whereas a grid resolution of 6 cells across the gap between inner and outer cylinder proved to be sufficient for the concentric configuration Scurtu et al. [3] the eccentric case demanded at least 8 cells. The result of this test case is shown in Fig. 5 where the effect of eccentricity on the critical Reynolds number is plotted.

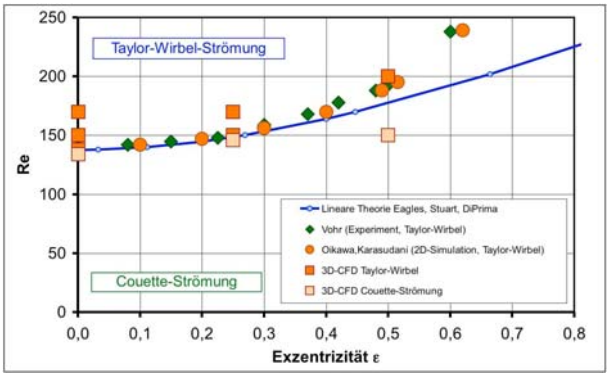

Fig. 5: stability of the Couette flow: critical Reynolds number vs. eccentricity, Ψ = 10%, experimental data Vohr [4], linear theory by Eagles et al. [5], 2D simulation by Oikawa et al. [6].

Perić [7] recommended a finer grid structure over a higher order of the solver, to avoid the risk of artificial numerical effects. Both, Perić' recommendation and our own results led to the selection of 12 cells to build the minimum gap width. Furthermore, the grid generation was most efficient when hexagonal cells were used. With a minimal number of defects and acceptable computing time the gap was filled with a block-structured grid combined with an O-grid for the feedhole section. An example of the grid for Ψ =2.5% and ε = 0.9 is given in Fig. 6.

However, one consequence pertaining to the necessity to use 12 cells across the gap is the need to take stretched cells in order to keep the total number of grid elements below 10^6. The enlarged section of the grid in the upper right hand corner in Fig. 6 gives an impression of the cell shape. A parameter to characterize the stretching of a cell is the aspect ratio, which is defined as the average side area divided by the normalized volume of the cell. This parameter can be found in Nobis and Schmidt [8], who carried out an extensive study to optimize computation performance by varying grid parameters such as A_R and the total number of cells in the computational domain.

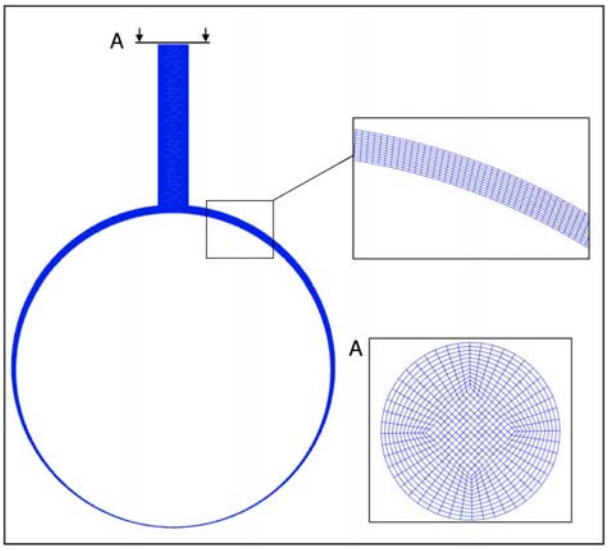

Fig. 6: computation grid for Ψ = 2.5% and ε = 0.9

$$A_R = \frac{\frac{1}{6}\sum_{i=1}^{6} A_i}{\sqrt[3]{V^2}} \qquad (12)$$

In general A_R takes values between 1 (cube) and a maximum of 10. The higher A_R the smaller becomes the grid size but at the same time the distortion of the cell increases, which in turn requires more iteration cycles. An acceptable compromise between computation time due to the total number of cells and iteration cycle was found for this flow case for $A_R = 6$.

2.3 Engine parameters

In addition to the feedhole position (Fig. 1) the oil supply flow rate itself is a second important parameter. Literature research produced several sources, which are combined in Fig. 7 where the normalized oil flow α according to equation (13) is plotted over the dimensionless bearing width γ.

$$\alpha = \frac{Q_{in}}{\frac{1}{2}U_1 B H_0} \qquad (13)$$

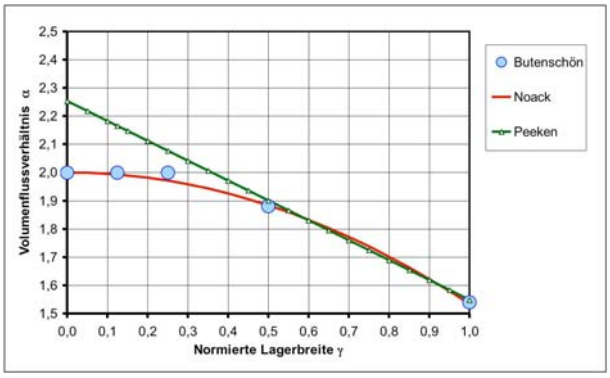

Fig. 7: oil supply flow rate vs. bearing width for ε = 1.0, according to Butenschön [9], Noack [10] and Peeken [11].

The standard width for main bearings in automotive applications is about 25% of the nominal bearing diameter (i.e. γ = 0.25). Hence, the recommended oil flow rate is up to 2 and the values of α selected for the work in progress are ranging from 1.0 to 2.0 covering smaller values of ε starting at 0.9.

2.4 Validation experiment

A continuous verification of CFD results by means of a validation experiment has proved to be successful during the development of this project. This constant exchange of results between experiment and simulation did result in improvements in both, the experimental apparatus, which is displayed in Fig. 8 and the numerical methods as the example regarding the effect of the eccentricity on the critical Reynolds number has shown earlier.

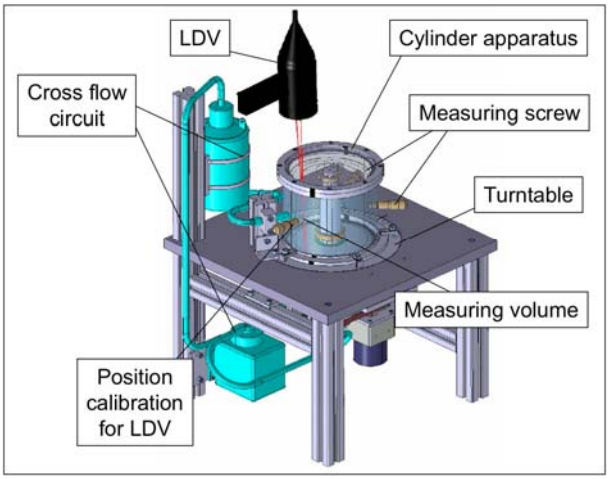

Fig. 8 experimental apparatus with two independently rotating cylinders, cross flow system and LDV

The apparatus has been continuously upgraded and the current version was designed by Vaczi [12]. Detailed results pertaining the vortex distribution inside the gap in relation to the gap size, Reynolds number and eccentricity are discussed in Nobis et al. [13].

With respect to the three-dimensional structure of the flow in the vicinity of the feed hole the focus must be on velocity profiles. As an example of the many data available in Fig. 9 upstream and downstream velocity profiles are plotted, which demonstrate the excellent consistency that was ultimately reached after refining the simulation methods and upgrading the experiment.

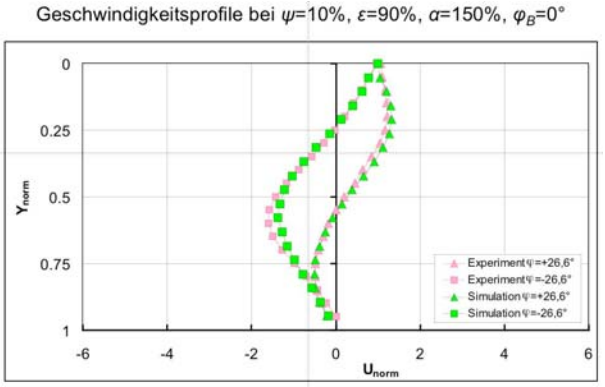

Fig. 9 profiles of the circumferential velocity upstream and downstream of the feedhole for flow rate α = 1.5, Ψ = 10% and ε = 0.9, LDV and CFD results.

3. Results

The very complex structure of the flow field of the lubrication film is illustrated in Fig. 10, which shows basically three layers that are stacked across the gap. Attached to the inner cylinder the circumferential main flow is found, which is driven by the rotation of the inner cylinder. The fluid emerging from the feedhole forms the middle layer, which is evolving into a torus-shaped vortex surrounding the feed hole. The third layer is composed by the re-circulating flow, which fills most of the volume in the wide gap region surrounding the incoming flow rate and its vortex.

Fig. 10 streamlines of the incoming flow in the vicinity feedhole for flow rate α = 1.0, Ψ = 10% and ε = 0.9, numerical simulation.

The velocity vector plot of the axial cross section reveals further details of the flow field, which are displayed in Fig. 11.

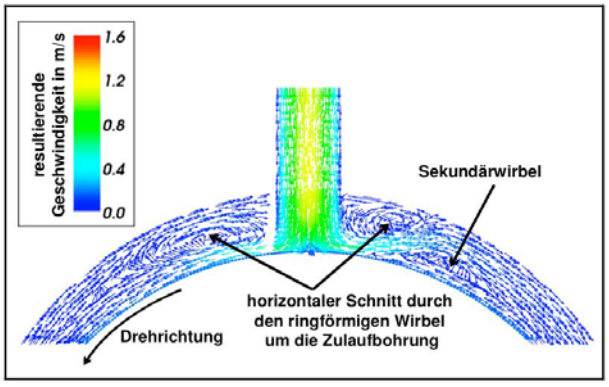

Fig. 11 velocity vector plot in the axial cross section through the feedhole for flow rate α = 1.0, Ψ = 10% and ε = 0.9, numerical simulation.

The torus vortex is visible surrounding the feedhole and upstream a secondary vortex is found in between the reversed flow and the main flow attached to the inner cylinder. These structures are typical for wider gaps. For a narrower gap (Ψ = 2.5%) the strength of the torus vortex decreases and the incoming flow surges strongly upstream into the region of reversed flow, which is shown in the following Fig. 12.

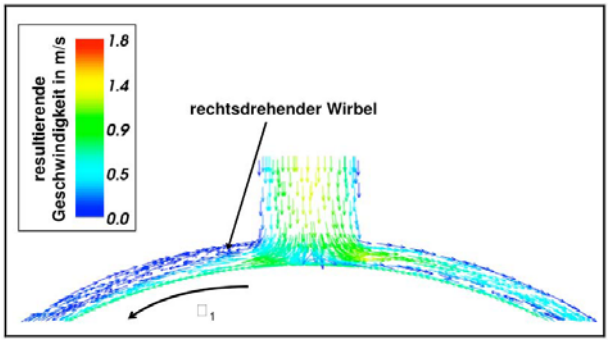

Fig. 12 velocity vector plot in the axial cross section through the feedhole for flow rate α = 1.0, Ψ = 2.5% and ε = 0.9, numerical simulation.

The strong upstream flow, which almost jet-like of the incoming flow becomes stronger with increasing flow ration α, which is illustrated by Fig. 13 and indicated by the red colored arrows.

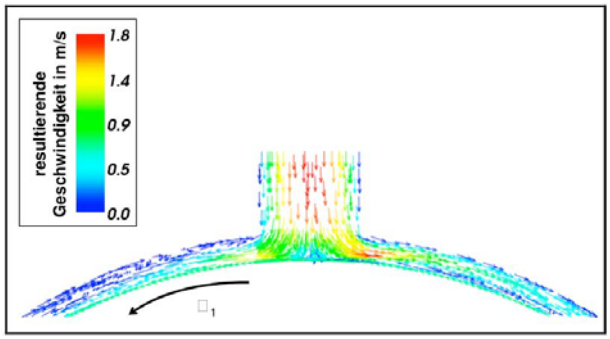

Fig. 13 velocity vector plot in the axial cross section through the feedhole for flow rate α = 1.5, Ψ = 2.5% and ε = 0.9, numerical simulation.

The Figures 11 through 13 clearly show the complex nature and three-dimensionality of the flow inside the lubrication film of a hydrodynamic journal bearing. Depending on key parameters like gap width Ψ and flow rate α structural changes can be found. In larger gaps a torus shaped vortex defines the flow surrounding the feedhole. With decreasing gap width the strength of this vortex declines and the interaction between incoming flow and reversed flow becomes more dominant. Moreover, local flow separation is seen downstream of the feedhole.

4. Summary

Whereas the general design of hydrodynamic journal bearings make use of a simplified theory based on the two-dimensional Reynolds equation a full understanding of the flow inside the bearing can only be reached when a three-dimensional CFD methods based on the Navier-Stokes equations are used.

This paper presents such an approach. Extensive literature research provided the necessary input data e.g. geometrical dimensions and oil flow rate.

Strong emphasis was given to the design of the computational grid. In pre-studies the minimum number of cells was researched that is required to generate the necessary resolution describing the three-dimensionality of the flow inside the oil film.

Numerical results were evaluated with experimental data, which were obtained qualitatively by means of flow visualization to create an overall impression of the flow features and quantitatively by velocity measurements using LDV-technique to compare velocity profiles with a high spatial resolution.

Based on this extensive preparation the paper presents detailed information of the flow in hydrodynamic journal bearings. In the vicinity of the feedhole through which the oil flow rate is supplied into the lubrication film complex flow structures were found. A strong interaction between incoming flow, circumferential main flow near the shaft and reversed flow near the bushing were observed, which results in the formation of various vortex formations in relation to gap width and flow rate.

Future activities include the extension of the CFD calculation towards smaller gap sizes and the inclusion of a cavitation module to predict the generation and implosion of cavitation bubbles.

5. Nomenclature

Symbol	Definition	Quantity
A		side area of control volume
A_R	eq. (12)	aspect ratio
B		nominal bearing width
D_1	$2R_1$	nominal bearing diameter, shaft diameter
H_0	$R_2 - R_1$	nominal gap width
Q_0	$\frac{1}{2}U_1 B H_0$	main flow rate
Q_{in}		supply flow rate
R_1		radius shaft, inner cylinder
R_2		radius bushing, outer cylinder
U_1	$\omega_1 R_1$	circumferential speed of shaft
V		Volume
d_B		feedhole diameter
e		eccentricity
h	$H_0(1+\varepsilon\cos\varphi)$	local gap width
p		pressure
r,x,y,z		coordinates
u,v,w		velocity components
α	eq. (13)	dimensionless flow rate
γ	$\frac{B}{D_1}$	dimensionless bearing width
ε	$\frac{e}{H_0}$	dimensionless eccentricity
μ		dynamic viscosity
ν		kinematic viscosity
ρ		density
φ		angle
φ_B		angular position of feedhole
ψ	$\frac{H_0}{R_1}$	dimensionless gap width
ω_1		angular velocity of shaft

6. Abbreviations

Symbol	Full spelling
CFD	Computational flow dynamics
EHD	Elasto-hydrodynamics
FEM	Finite element method
LDV	Laser Doppler velocimeter

7. References

[1] M. Berg: Verbrennungsmotoren-Gleitlager, Tutorial script, Westsächsische Hochschule, Zwickau. 2004.

[2] H. Gläser: Schäden an Gleit- und Wälzlagerungen, Verlag Technik GmbH, Berlin. 1990.

[3] N. Scurtu, P. Stücke, C. Egbers: Numerical and experimental study of the flow in an eccentric Couette-Taylor system with small gap. PAMM, Vol. 8, Issue 1, pp 10641 – 10642. 2008.

[4] J. H. Vohr: An experimental study of Taylor vortices and turbulence in flow between eccentric rotating cylinders. Trans. ASME, J. Lubrication Tech. 90, 285-296. 1968.

[5] P.M. Eagles, R.C. Di Prima, J.T. Stuart: The effects of eccentricity on torque and load in Taylor-vortex flow. J. Fluid Mech. 87, part 2, 209-231. 1978.

[6] M. Oikawa, T. Karasudani, M. Funakoshi: Stability of flow between eccentric rotating cylinders. J. Phys. Soc. Japan 58, No. 7, 2355-236. 1989.

[7] Milovan Perić: Analyse der Genauigkeit numerischer Strömungsberechnung in Kurzlehrgang Strömungsmaschinen, LSTM Universität Erlangen. 2009.

[8] M. Nobis, M. Schmidt: Experimentelle und numerische Untersuchung der Schmierspaltströmung. Master Thesis, Westsächsische Hochschule, Zwickau. 2009.

[9] H.-J. Butenschön: Das hydrodynamische, zylindrische Gleitlager endlicher Breite unter instationärer Belastung. Diss. TU Karlsruhe. 1976.

[10] G. Noack: Berechnung hydrodynamisch geschmierter Gleitlager — dargestellt am Beispiel der Radiallager; Gleitlager als moderne Maschinenelemente; Tribotechnik Bd. 400. Ehningen, Expert-Verlag. 1993.

[11] H. Peeken: Dynamisch belastetes Gleitlager, Schmierspaltfüllung: Abschlussbericht. Rheinisch-Westfälische Technische Hochschule Aachen, Lehrst. f. Elast. DFG Bonn, Aachen. 1985.

[12] T. Vaczi: Konstruktive Überarbeitung eines Zylinderspaltapparates und Untersuchung der exzentrischen Zylinderspaltströmung bei verschiedenen Streckungsverhältnissen. Diploma Thesis, Westsächsische Hochschule, Zwickau. 2008.

[13] M. Nobis, M. Schmidt, P. Stücke, N. Scurtu, C, Egbers: 3D-Strömungsstruktur in engen Zylinderspalten mit Exzentrizität und Seitenfluss. GALA, 17th Annual Conference, Erlangen. 2009.